

RSC Advances



This is an *Accepted Manuscript*, which has been through the Royal Society of Chemistry peer review process and has been accepted for publication.

Accepted Manuscripts are published online shortly after acceptance, before technical editing, formatting and proof reading. Using this free service, authors can make their results available to the community, in citable form, before we publish the edited article. This *Accepted Manuscript* will be replaced by the edited, formatted and paginated article as soon as this is available.

You can find more information about *Accepted Manuscripts* in the [Information for Authors](#).

Please note that technical editing may introduce minor changes to the text and/or graphics, which may alter content. The journal's standard [Terms & Conditions](#) and the [Ethical guidelines](#) still apply. In no event shall the Royal Society of Chemistry be held responsible for any errors or omissions in this *Accepted Manuscript* or any consequences arising from the use of any information it contains.

ARTICLE

A Novel Approach to Prepare Graphene oxide/Soluble Polyimide Composite Films with Low Dielectric Constant and High Mechanical Properties

Cite this: DOI: 10.1039/x0xx00000x

Received 00th January 2012,
Accepted 00th January 2012

DOI: 10.1039/x0xx00000x

www.rsc.org/

Wei-Hao Liao, Shin-Yi Yang, Sheng-Tsung Hsiao, Yu-Sheng Wang,

Shin-Ming Li, Hsi-Wen Tien, Chen-Chi M. Ma*^a and Shi-Jun Zeng

This paper proposes an effective and simple approach to fabricate high-performance graphene oxide (GO)/soluble polyimide (SPI) composite films through a novel and effective process. In this method, GO is dispersed in a dissolved SPI (R-SPI) polymeric matrix with curing state, preventing the reduction of crosslinking reactions of the polymeric matrix, and resulting in substantial improvements in the mechanical and dielectric properties of the composite. The GO/R-SPI composite film contains only 1.0 wt% GO; it possesses high tensile strength (up to 288.6 MPa) and Young's modulus (7.58 GPa), which represent an increase of 260% in tensile strength and 402% in Young's modulus, compared with the neat SPI film (80.3 MPa and 1.51 GPa, respectively). The dielectric constant (D_k) decreases with an increase in the GO content; the D_k of the GO/R-SPI composite film can be as low as 2.1 (compared with 2.8 for the neat SPI film). This novel fabricating method provides a path for developing high-performance GO/R-SPI composite materials as next-generation low-k dielectric materials.

1. Introduction

Ultra-large-scale integration (ULSI) processes have been used to minimize the dimensions, and to enhance the integration density of integrated circuit (IC) devices. The number of interconnects in ICs is continually increasing, resulting in electronic signal interference (noise, crosstalk, and power dissipation) by parasitic resistance and capacitance delays (RC delay)¹. Equation (1) illustrates the relationship among the key factors.²⁻⁴

$$RC(\tau) = 2\rho\epsilon_r \left[\frac{4L^2}{P^2} + \frac{L^2}{T^2} \right] \quad (1)$$

Where

- ρ : The resistance of metal electronic wire.
- ϵ_r : The relative permittivity of interlevel-metal insulator.
- L : The length of metal electronic wire.
- T : The height of metal electronic wire.
- P : The distance between two metal electronic wires.

Miniaturized dimensions and increasing complexity present a challenge to optimize devices by minimizing L and maximizing T and P. The signal transmission quality has been improved and the RC delay problem has been efficiently solved by reducing both ρ and ϵ_r ⁵. Copper is an optimal material for

metal electronic wires, thus developing a low-dielectric-constant material to provide an interlevel metal insulator, which is of interest to scientists and the semiconductor manufacturing industry³. The International Technology Roadmap for Semiconductors (ITRS) (2014) requires the interlayer dielectric (ILD) materials to have bulk dielectric constants (D_k) below 2.4, and possess tensile strength above 200 MPa for constructing IC structures^{1,5}.

Polymer-based ILD materials have attracted scientific and industrial interest because of their low cost and versatility^{2,6-8}. However, the electrical properties of these materials do not meet the current ILD requirements for ULSI multilevel interconnections. The most convenient method for decreasing the D_k is to construct materials with a porous structure⁶, because the D_k of air is approximately 1.0¹. However, the mechanical properties of porous materials are typically too weak for ILD material applications. Previous reports^{2,9} have proposed other approaches to reduce the dielectric constants of materials without sacrificing the mechanical properties, such as (1) designing the material molecular structure to incorporate fluorine-containing groups, and (2) incorporating insulating nanofillers in the matrix.

Polyimides (PIs) possess high thermal stability, excellent mechanical properties, favorable chemical resistance, and unique dielectric properties with D_k values in the range of 3.2–

3.9¹⁰. Consequently, PIs have been used in the electronics industry, and also in aerospace applications, automobiles, adhesives, nonlinear optical devices, and liquid crystal display applications^{11–15}. In addition, soluble polyimides (SPIs) incorporate symmetrically placed fluorine-containing functional groups within their chemical structures, and these groups efficiently reduce the dielectric constant to values in the range of 2.6–2.8. Thus, SPIs have great potential as low- D_k matrix materials^{1, 11, 16}. PI composites with nanofillers have generated considerable industrial and academic interest because they exhibit multifunctional and valuable properties. By using PIs for fabricating organic–inorganic hybrid materials such as silica/PI¹⁷, clay/PI¹⁸ and POSS/PI¹⁹, the mechanical properties of PI can be improved, and the dielectric constant can be reduced.

For various nanofillers, graphene-based nanomaterials provide an alternative multifunctional composite material with superior properties, and their basic material, graphite, possesses a large natural abundance²⁰. Graphene-based materials, such as graphene nanosheets (GNS) and graphene oxide (GO), can enhance the properties of polymer composite materials, because of their extraordinarily high surface area, unique electrical properties, graphitized planar structure, and low manufacturing costs^{21, 22}. The chemical structure of GO differs greatly from that of GNS, providing a 2D sheet of covalently bonded carbon atoms bearing various oxygen functional groups (e.g., hydroxyl, epoxide, and carbonyl groups) on the basal planes and at the edges. These oxygen-containing groups on the GO surface provide electrical insulation, and improve the compatibility and dispersion of polymeric matrices^{23, 24}. Recently, the GO/PI composites have been studied on various properties^{1, 25–27}. However, there are few reports on the application of GO-based nanofiller as a dielectric-reinforcement material in polymeric composites.

Conventional processes for fabricating GO/PIs composites involve two steps, as follows: First, GO is dispersed in poly(amic acid) (PAA) before imidizing condensation; a high-temperature process is then performed to imidize the PAA and remove the solvent. This conventional process for fabricating GO/PI composites is inconvenient and ineffective. Because the dispersed GO in PAA before imidization can cause an obvious increase in viscosity and steric hindrance, the dispersibility of the GO sheets in PIs might be limited, and the crosslinking reaction of the polymeric matrices might be reduced (low crosslinking density), further reducing the reinforcing efficiency of GO-based nanofillers^{25–29}. Hence, developing a simple and effective method for fabricating GO-based composites is crucial.

This paper proposes a simple, practical, and effective approach to prepare high-performance GO/SPI composite films through a dissolved method. In this method, the pre-synthesized SPI (uniform crosslinking density) is first dissolved in an organic solvent; the GO sheets are then homogeneously dispersed in the SPI solution because of their high affinity with the solvent. Consequently, the GO/dissolved SPI (R-SPI) solution exhibits excellent dispersion of the GO sheets, and the

organic solvent can be conveniently removed through vacuum at a low temperature (approximately 100 °C) to fabricate GO/R-SPI composite films (as shown in Fig. 1). Compared with the GO/SPI composite films prepared using the conventional solution-blending method, the GO/R-SPI films exhibited a considerable improvement in mechanical and dielectric properties for a given GO content, indicating that dispersed GO in a polymeric matrix without the steric hindrance of the GO sheets restraining the crosslinking reactions of the host polymer. Furthermore, this study also demonstrated that the D_k values of the GO/R-SPI films exhibited a substantial decrease to just 2.1, suggesting that this approach provides a promising path for developing high-performance GO/SPI composite materials as next-generation low- k dielectric materials.

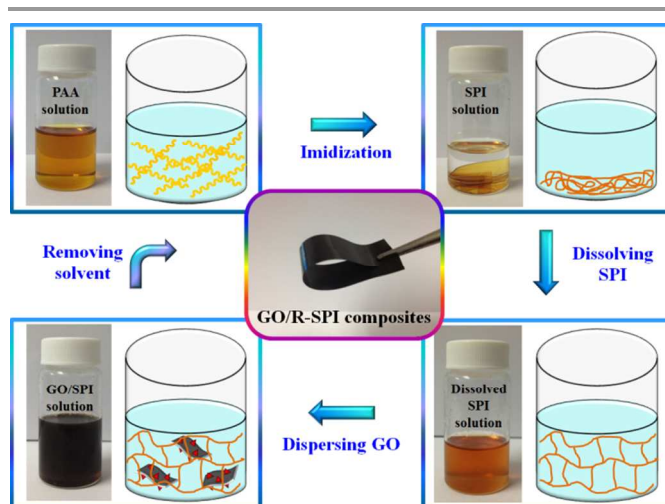


Fig. 1 The proposed processes of the GO/R-SPI composite films.

2. Experimental section

2.1 Materials

2,2-bis(3,4-dicarboxyphenyl)hexafluoropropane dianhydride (6FDA) was purchased from Aldrich Chemical Company, St. Louis, MO, USA. 4,4-diaminodiphenyl ether (ODA) was obtained from TCI America, Portland, Oregon, USA. Nano Graphites (NGPs) were supplied by Angstrom Materials LLC, Dayton, OH, USA, which were produced by a chemical vapor deposition (CVD) process. The thickness of the NGPs was thinner than 100 nm. Potassium permanganate (KMnO_4), sodium nitrate (NaNO_3), dimethylacetamide (DMAc), and sulfuric acid (H_2SO_4) were received from the Showa Chemical Co., Tokyo, Japan.

2.2 Preparation of GO

On the basis of modified Hummers' method,³⁰ H_2SO_4 (50 mL) was poured into a 250 mL three-neck flask and stirred in an ice bath and the temperature was maintained at 0 °C. NGPs (2 g) and NaNO_3 (1 g) were added and stirred uniformly. KMnO_4 (6 g) was added slowly to the mixture in the reaction vessel with an ice bath over 30 min. The solution was heated to

35 °C and the oxidation was allowed to proceed for 24 h. Then, distilled water was added slowly, and the temperature was controlled below 100 °C. This reaction was terminated by adding a large amount of distilled water and 30% H₂O₂ solution (6 mL). The mixture was filtered and washed with distilled water. This process was repeated at least ten times until the pH of the percolated solution reached 7. The sample of GO was obtained after drying in a vacuum oven.

2.3 Preparation of GO/SPI composite films by solution blending method

To synthesize PAA, 1.0 g of ODA (5 mmol) was placed in a three-neck flask containing 15 mL of DMAc under nitrogen purge at room temperature. After ODA was completely dissolved in DMAc, 2.2 g of 6FDA (5 mmol) was divided into four batches, and each batch was then added to the three-neck flask every 1 h. After 6FDA was completely dissolved in DMAc, the solution was stirred for 2 h, and a viscous PAA solution was obtained. To prepare GO/PAA solutions in DMAc at different concentrations, various weights of GO (0.016, 0.032, and 0.048 g) were added to 10 mL of DMAc, individually, and each sample was then dispersed in DMAc through sonication. The dispersed GO suspensions were then mixed with PAA to prepare GO/PAA mixtures through blending in DMAc. These GO/PAA mixtures were poured into a glass dish, and were subsequently placed in a vacuum oven at 30 °C for 48 h before the imidizing condensation was performed. For imidizing the GO/PAA mixtures, the samples were placed in a convection oven at 100, 150, 180, and 230 °C for 2 h, and then at 300 °C for 5 min. Fig. 2(a) depicts the procedure for preparing the

GO/SPI films. The thickness of the GO/SPI films was approximately 0.1 mm.

2.4 Preparation of GO/R-SPI composite films through dissolved and dispersed process

One gram of ODA (5 mmol) was placed in a three-neck flask containing 15 mL of DMAc solvent under nitrogen purge at room temperature. After ODA was completely dissolved in DMAc, 2.2 g of 6FDA (5 mmol) was divided into four batches, and each batch was then added to the three-neck flask every 1 h. After 6FDA was completely dissolved in DMAc, the solution was stirred for 2 h, and a viscous PAA solution was obtained. This PAA mixture was poured into a glass dish, and was subsequently placed in a vacuum oven at 30 °C for 48 h before the imidizing condensation was performed. For imidizing the PAA mixtures, the samples were placed in a convection oven at 100, 150, 180, and 230 °C for 2 h, and then at 300 °C for 5 min. The neat SPI was added to DMAc (15 mL). Various weights of GO (0.016, 0.032, and 0.048 g) were individually dispersed in anhydrous DMAc (10 mL), through sonication (1 h), resulting in homogeneously dispersed GO sheets in the solution. After SPI was completely dissolved in DMAc (R-SPI), and the GO solution was added to the R-SPI solution, the GO sheets were dispersed through sonication (1 h). To prevent the reduction of the oxygen-containing functional group on the GO surface, a vacuum process was used at 100 °C for 3 h to remove the DMAc. Fig. 2(b) depicts the procedure for preparing GO/R-SPI films. The thickness of the GO/R-SPI films was approximately 0.1 mm.

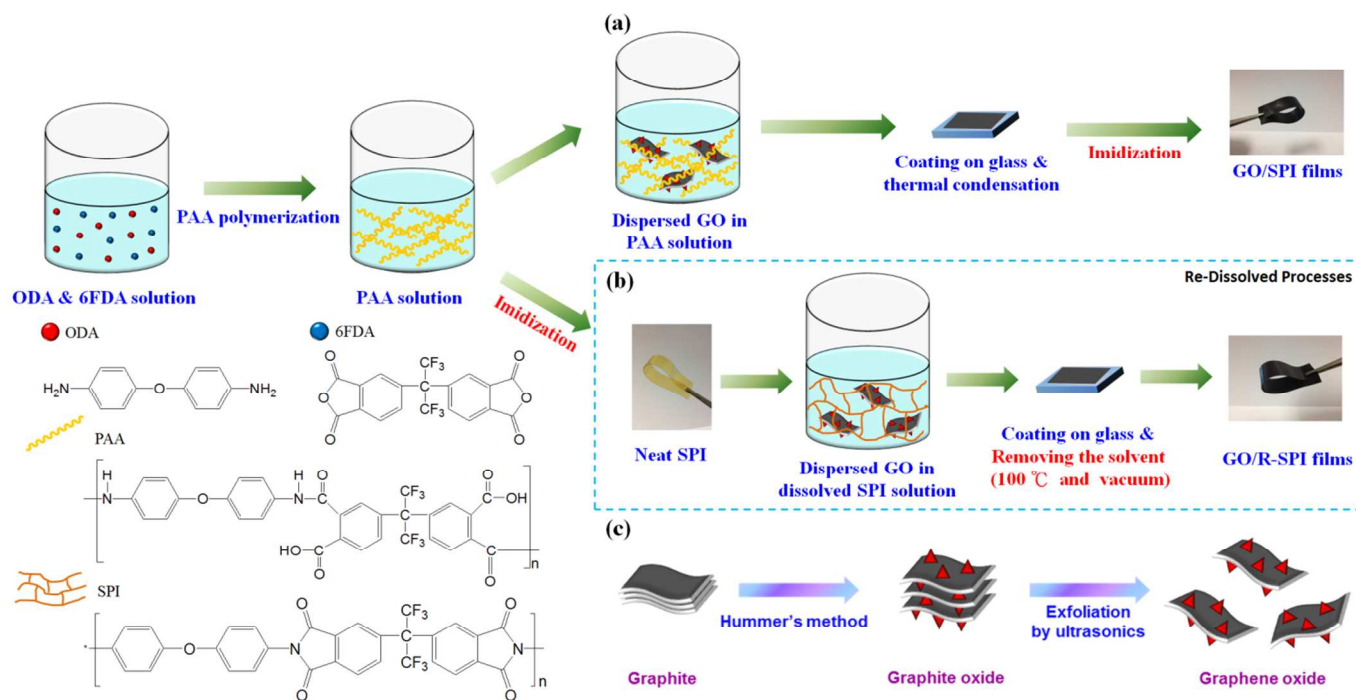


Fig. 2 Scheme of the procedure for preparation of (a) GO/SPI films, (b) GO/R-SPI films and (c) GO sheets.

2.5 Characterization and Instruments

The scanning electron microscope (SEM) used in this work was a Hitachi S-4200 SEM (Hitachi Limited, Tokyo, Japan) with an accelerating voltage of 15 kV. A high resolution X-ray photoelectron spectrometer (XPS) (ESCA PHI 1600, Physical Electronics, Lake Drive East, Chanhassen, MN, USA) was used to detect the presence of surface elements. An Ultima IV multipurpose X-ray diffraction (XRD) system (Rigaku Co., Sendagaya, Shibuya-Ku, Tokyo, Japan) was used for the X-ray analysis with Cu-K α radiation ($\lambda=1.54051 \text{ \AA}$). Step scanning was used with 2θ intervals from 2° to 40° with a residence time of 1s. The topography of GO was identified by an atomic force microscope (AFM, Digital Instrument D3100, New York, USA). Transmission electron microscope (TEM) observations were conducted using a JEM-2100 microscope (JEOL Limited, Tokyo, Japan) with 200 kV. Thermogravimetric analyses (TGA) were performed with a Du Pont TGA 2900 analyzer from 30 to 800 $^\circ\text{C}$ in nitrogen (N_2) at a heating rate of 10 $^\circ\text{C}/\text{min}$. The curing processes of the PAA/GO (the solvent had been removed) composites were investigated by a differential scanning calorimeter (DSC, TA Instruments Q600, Utah, USA) in the temperature range from 30 to 250 $^\circ\text{C}$ with a heating rate of 10 $^\circ\text{C}/\text{min}$ in nitrogen atmosphere. To measure the tensile strength and modulus of the SPI films, samples were cut to sheets with a width of 10 mm, and were tested using an Universal Testing Machine (Tinius Olsen H10K-S Benchtop Testing Machine, Horsham, PA, USA). The test procedure was followed the ASTM-D882. Dimensions of test specimen were 50mm \times 5mm \times 0.1 mm; the crosshead speed was 5 mm min^{-1} . The dielectric constants of GO/SPI and GO/R-SPI films were measured over a frequency range from 0.01 to 1.0 GHz at room temperature using a dielectric spectrometer (Hewlett Packard 4291A RF Impedance Analyzer, Palo Alto, California, USA).

3. Results and discussion

3.1 Characterization of GO

Fig. 3(a) shows the TEM micrograph, which illustrates the morphology of GO. The GO surface presented a high density of oxygen-containing functional groups, consequently, GO exhibited a smooth carpet-like structure. GO possessed unique 2D nanostructures that differed from the structures of carbon black or graphite. GO-based materials exhibit large aspect ratios that enhance their contact areas within the polymeric matrix; this is a crucial factor for the performance improvement of the GO-containing polymeric composites.

The GO surface morphologies were elucidated using AFM; Figs. 3(b) and 3(c) illustrate the topography and cross-sectional view of GO, respectively. The samples used for AFM studies were prepared by depositing the corresponding dispersions onto a silicon wafer, and drying in a vacuum at room temperature. The GO sheet exhibited a smooth surface with few wrinkles. The cross-sectional view of the exfoliated GO revealed that the GO sheets exhibited an average thickness of approximately

1.3 nm. Similar AFM observations have been reported^{31, 32}, and indicated that the thickness was single-layered GO.

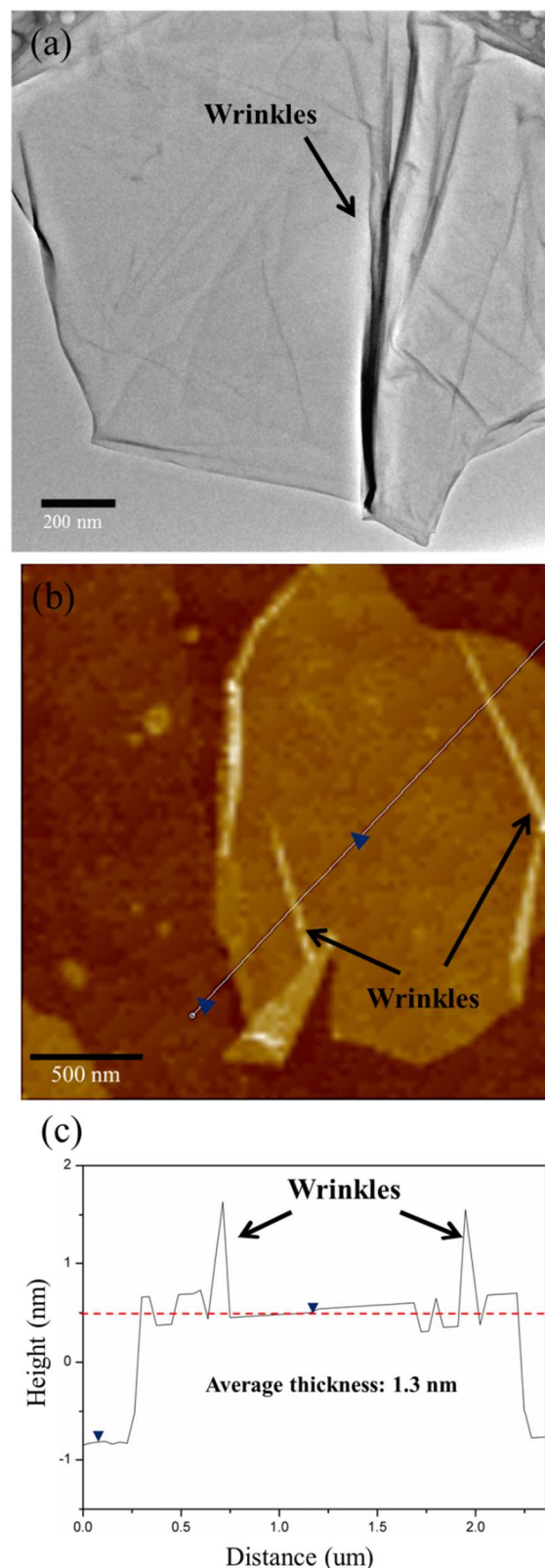


Fig. 3 (a) TEM images of GO; (b) tapping mode AFM images of exfoliated GO; (c) cross-sectional view of GO.

Fig. 4 shows the XRD spectra of the graphitic (002) faces of graphite and GO. The XRD pattern of graphite shows a sharp diffraction peak at approximately $2\theta = 26.6^\circ$, corresponding to an interlayer spacing of 0.34 nm. The GO was prepared from graphite by using the modified Hummers method,³⁰ its diffraction peak (002) significantly shifted to a smaller angle region ($2\theta = 10.3^\circ$, corresponding to an interlayer spacing of 0.86 nm), and the peak intensities were reduced. These changes indicated that oxygen-containing functional groups had incorporated into the exfoliated GO sheets to increase the interlayer distances and structural heterogeneity. The presence of oxygen-containing functional groups on the GO surface can hinder the restacking of planar GO nanosheets, and thus, induce ordered graphitic stacking to disordered structures. The increased interlayer spacing indicated that the graphite was completely transformed into GO, and that most of the oxygen was bonded to the GO surface.

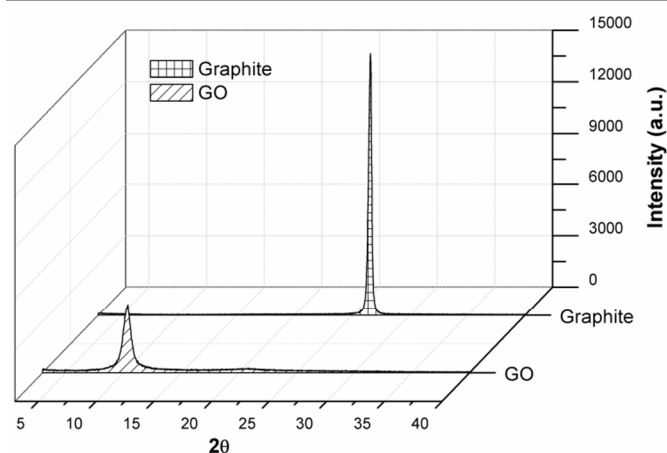


Fig. 4 XRD patterns of graphite and GO.

The XPS spectra were analyzed to elucidate the surface composition of graphite and GO. XPS survey scans of GO and graphite were conducted to determine the elemental composition of the sample surface; the resulting spectra of graphite and GO are shown in Fig. 5(a). GO exhibited a substantially more intense O1s peak than that of graphite. This increase in signal intensity resulted from the presence of oxygen-containing groups on the GO surface, and the C/O atomic ratio changed from 89:11 in graphite to 67:33 in GO, and thus confirmed that the modification was successful.

A detailed analysis of the XPS C1s spectra of graphite and GO (Figs. 5(b) and 5(c)) revealed a substantial degree of oxidation on the GO surface. The spectra of graphite exhibited peaks from sp^2 carbon atoms (284.3 eV) in aromatic rings and single-bonded sp^3 carbon atoms (284.9 eV). The intensity of the peak at 284.3 eV was stronger than that of the peak at 284.9 eV because an additional $\pi-\pi^*$ transition was present at 291.1 eV, which arose from delocalized electrons in an aromatic network of graphite^{2, 25, 33}. The spectra indicated the presence of small quantities of various oxygen-containing groups on the graphite surface. After oxidation, the intensity of the sp^2 peak at 284.3 eV was lower than that of the sp^3 carbon peak at 284.9 eV,

and the $\pi-\pi^*$ peak at 291.1 eV was no longer present. GO presented a substantial degree of oxidation, evidenced by numerous peaks in the XPS spectra representing oxygen functionalities such as C–OH (285.6 eV), C–O–C (286.8 eV), COOH (287.8 eV), and C=O (289.0 eV)^{33, 34}.

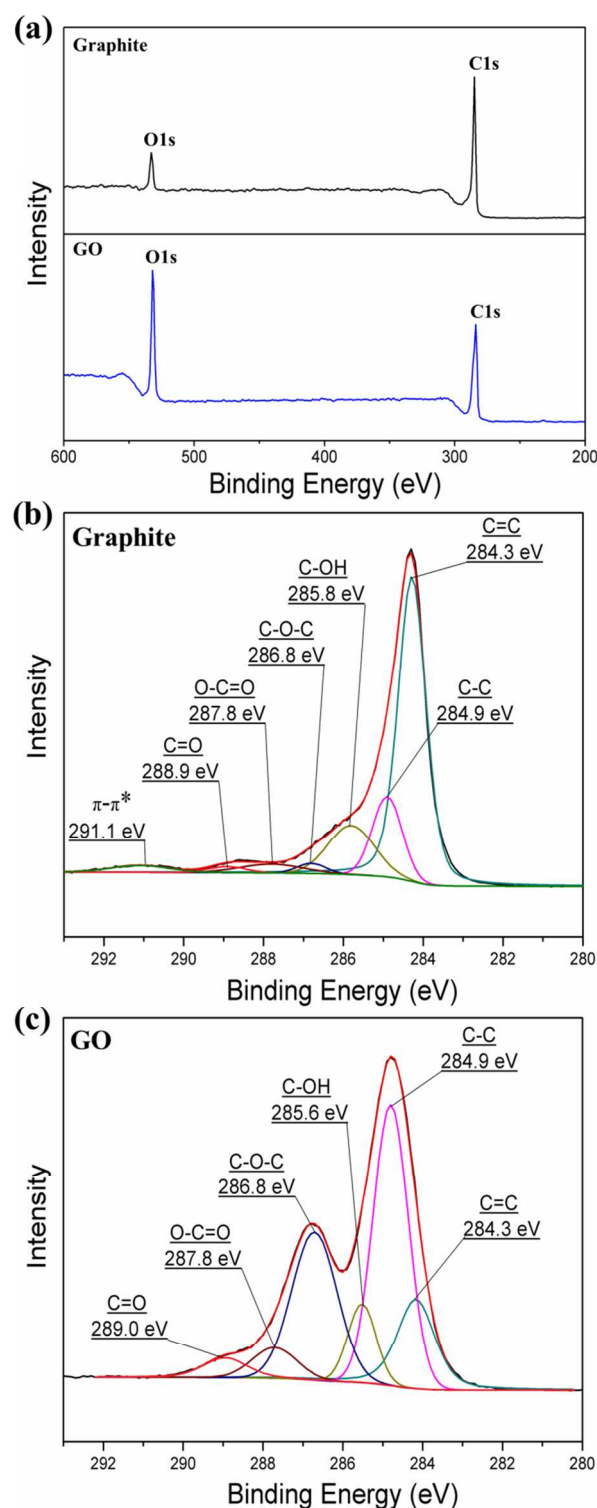


Fig. 5 (a) XPS survey scans of graphite and GO; High resolution C1s XPS spectrum of (b) graphite and (c) GO.

TGA is a useful tool for investigating the quantity of oxygen-containing substances on graphene. Fig. 6 shows the representative TGA thermograms which illustrate the loss of weight that graphite and GO during heating. For graphite, only a small loss in weight occurs below 800 °C because of its excellent thermal stability.²⁵ However, GO undergoes significant weight loss between 125 and 325 °C, which results from the reduction of oxygen-containing functional groups. GO incurs a small additional weight loss between 325 and 800 °C due to the defects, such as disordered and amorphous carbon, in the graphene structure.^{25, 35} From the TGA results, the weight fraction of the oxygen-containing substances on GO can be estimated as approximately 42.2 wt%, indicating that the oxidization of graphene was successful.

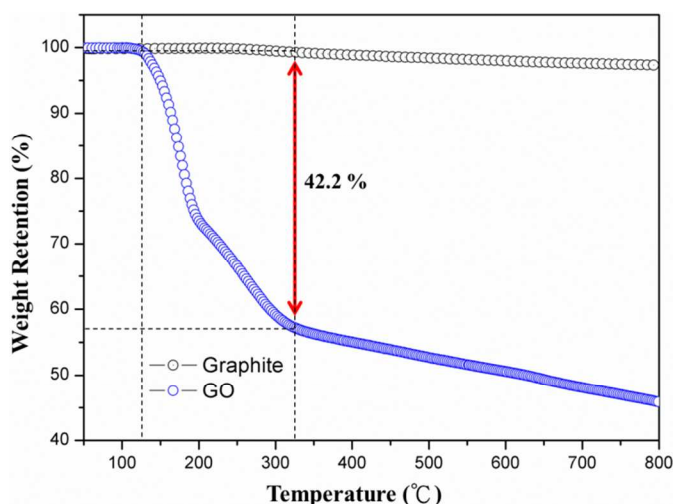


Fig. 6 TGA curves of graphite and GO with a heating rate of 10 °C/min in N₂.

In summary, the results from AFM, TEM, XRD, XPS, and TGA clearly confirmed that preparing GO sheets by using the modified Hummers method was successful. GO was dispersed in the R-SPI polymeric matrix to fabricate GO/R-SPI composite materials, and was expected to enhance the mechanical properties and decrease dielectric properties of the materials, compared with those of composites fabricated by blending GO at the PAA solution.

3.2 Thermal properties of GO/PAA composites

DSC is a powerful technique for determining the thermodynamic properties of a polymeric matrix. Because the crosslinking reaction of PI is an exothermic reaction, we estimated the enthalpy of crosslinking reaction by the exothermic peak from the DSC curves of GO/PAA composites²⁵. The enthalpy of PI crosslinking reaction is larger, and the crosslinking density of polymeric matrix is higher^{25, 27, 28}. A comparison of the DSC curves of the GO/PAA composites (as shown in Fig. 7) provided an indication of the degree of crosslinking in the GO/SPI composites. The DSC curves of the imidization of PAA to SPI exhibited an exothermic peak in the range of 125–220 °C³⁶. The enthalpy and exothermic peak temperature can be estimated from the

exothermic peaks, using the Universal Analysis 2000 software (TA Instruments). This study determined that increasing the GO content in the PAA matrix lowers the crosslinking density of SPI. The enthalpy change of 1.5 wt% GO/PAA during curing (64.27 J/g) was significantly less than that of neat PAA (74.41 J/g). The exothermic peak temperature shifted from 166.8 °C for neat PAA to 180.5 °C for 1.5 wt% GO/PAA. These results confirmed that introducing GO nanosheets with a high surface area into the PAA matrix caused a steric hindrance to influence the crosslinking reaction. Moreover, aggregated and restacked GO can also interfere with the crosslinking reaction. Consequently, the presence of GO increases the PAA viscosity and reduces the crosslinking reactivity during curing. This similar phenomenon has been reported by other researchers²⁵⁻²⁸. Thus, neat SPI, with dense and uniform crosslinking structure, was dissolved to disperse the GO sheets, and was then used to prepare GO/R-SPI composite films.

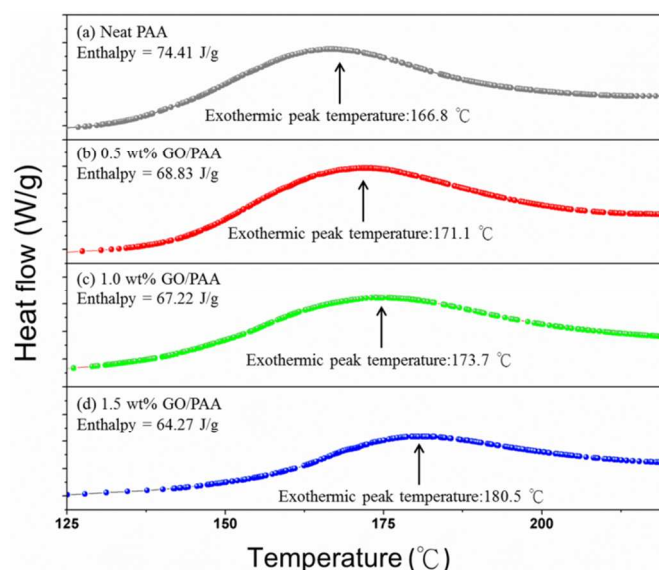


Fig. 7 The DSC exothermal peak of GO/PAA composites.

3.3 Mechanical properties of GO/SPI and GO/R-SPI films

To investigate the mechanical properties of the GO/SPI and GO/R-SPI films, the tensile moduli, tensile strengths, and elongations at break of composite films with various GO contents (0.5, 1.0, and 1.5 wt%) were compared. The results are summarized in Fig.8 and Table 1. Ten samples of each film were tested. The tensile modulus and tensile strength of the neat SPI films were 1.51 GPa and 80.3 MPa, respectively. Regarding the 1 wt% GO/SPI films, the tensile modulus increased to 4.82 GPa (an increase of approximately 210% compared with the neat SPI film), and the tensile strength increased to 136.2 MPa (representing an increase of 69.6% compared with the neat SPI film). The tensile modulus and tensile strength of the neat R-SPI films were 1.49 GPa and 80.1 MPa, respectively, and were comparable to the tensile performance of the neat SPI films. Regarding the 1 wt% GO/R-SPI films, the tensile modulus and tensile strength were 7.58 GPa and 288.6 MPa, respectively. Thus, the 1.0 wt%

GO/R-SPI film with GO exhibited an increase of approximately 402% in tensile modulus and a substantial improvement (approximately 260%) of tensile strength, demonstrating that the GO/R-SPI films efficiently promoted a load transfer from the polymer matrix to the GO sheets. This improvement on the performance might have been caused by the dense 3D network

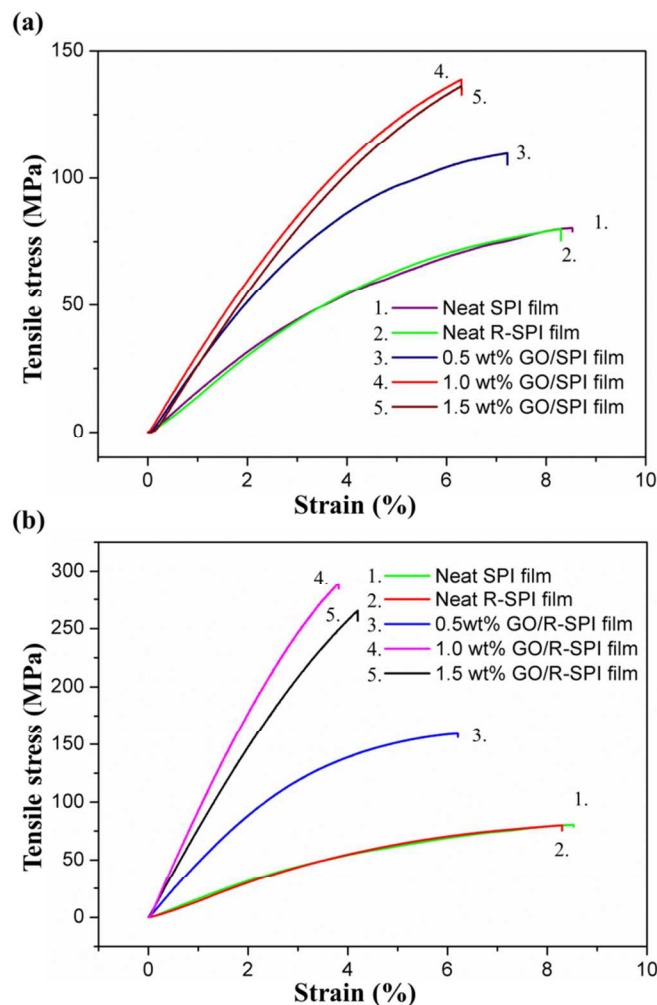


Fig. 8 Stress-strain curves of (a) GO/SPI and (b) GO/R-SPI composite films with various amounts of GO.

Table 1. Mechanical properties of GO/SPI and GO/R-SPI films.

Sample	Tensile modulus (Gpa)	Tensile strength (Mpa)	Elongation at break (%)
Neat SPI	1.51±0.08	80.3±2.2	8.5±0.3
0.5 wt% GO/SPI	2.94±0.18	109.6±1.8	7.2±0.2
1.0 wt% GO/SPI	4.82±0.26	136.2±2.1	6.3±0.4
1.5 wt% GO/SPI	4.58±0.25	128.5±2.9	6.5±0.5
Neat R-SPI	1.49±0.07	80.1±2.9	8.3±0.2
0.5 wt% GO/R-SPI	4.75±0.25	159.3±1.6	6.2±0.3
1.0 wt% GO/R-SPI	7.58±0.36	288.6±2.8	3.8±0.5
1.5 wt% GO/R-SPI	6.92±0.38	265.2±3.2	4.2±0.3

structure (high crosslinking density) of the polymeric matrix and the high contact surface area of GO within the R-SPI matrix. Furthermore, the stronger interfacial interaction between GO and R-SPI in the GO/R-SPI films, compared with that in the GO/SPI films, resulted from GO retaining a greater proportion of oxygen-containing groups during the lower temperature processes for preparing the GO/R-SPI composites. Therefore, the reinforcing efficiency of the GO/R-SPI films was considerably greater than that of the GO/SPI films. With a 1.5 wt% GO content, the tensile strength and tensile modulus of both GO/SPI films and GO/R-SPI films decreased slightly compared with that of the 1.0 wt% GO composites. When the GO filler reaches a critical content, the distance between sheets becomes sufficiently small. Therefore, the Van der Waals forces become very significant, and the GO sheets may be agglomerated, causing both a reduction in the aspect ratio of GO and the GO reinforcing efficiency. Therefore, it is important to optimize the GO content to maximize the mechanical properties of composite materials^{24, 37}.

Compared to the previous report³⁸, the GO/PI composites in our study exhibited the more obvious improvements on mechanical properties exactly. We conjecture that the difference in mechanical improvements between the previous report³⁸ and our study is affected by the GO loading in the PI matrix. Because the previous study³⁸ needed to maintain the GO/PI composites with transparency, those GO/PI composites in the previous report³⁸ incorporated with very low loading of GO, which is from 0.001 to 0.01 wt%. Relatively, our study investigated the GO/PI composites with the GO loading from 0.5 to 1.5 wt%.

3.4 Morphology of GO/SPI and GO/R-SPI films

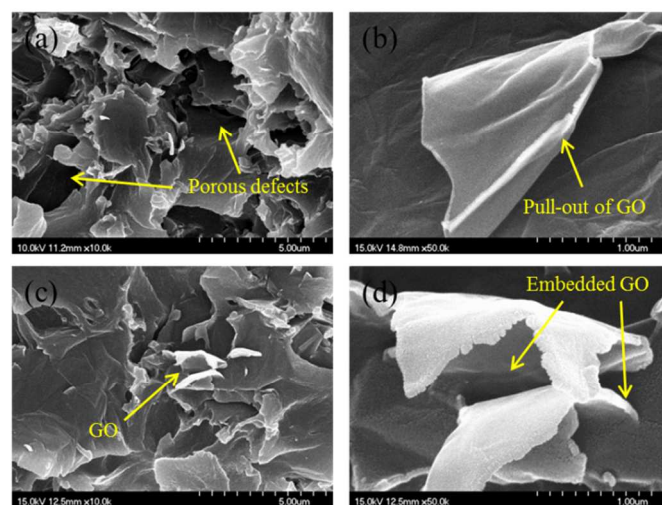


Fig. 9 SEM images of fractured surface of (a) 1.0 wt% GO/SPI film (x10k), (b) 1.0 wt% GO/SPI film (x50k), (c) 1.0 wt% GO/R-SPI film (x10k), and (d) 1.0 wt% GO/R-SPI film (x50k).

A high-resolution SEM was used to investigate the fractured surfaces of the GO/SPI and GO/R-SPI films (as shown in Fig. 9). SEM images of the GO/SPI films exhibited the heterogeneity, formation of defects, and significant roughness of the fractured surface. The porous defects may be caused by

the decomposed oxygen-containing groups on GO during high-temperature process. Furthermore, GO sheets were partially pulled out from the polymeric matrix. The results were attributed to the lower crosslinking density of the SPI matrix and the weak interfacial interaction between GO and SPI, which reduces the efficiency of load transfer from the polymeric matrix to the GO sheets. However, on the fractured surfaces of GO/R-SPI film, the GO sheets remained embedded in the polymeric matrix; thus, few defects were existed within the fractured surfaces. This result indicates that the GO/R-SPI films contain a complete 3D network (high crosslinking density) and possess stronger interfacial interaction between GO and the polymeric matrix than that of GO/SPI composites, which provides a dense SPI matrix to embed GO, transferring load from SPI matrix to GO. These SEM observations were consistent with the results of mechanical properties. Consequently, this study provides an effective method for maintaining crosslinking density of the SPI matrix during the fabrication of GO/R-SPI composite films.

3.5 Dielectric properties of GO/SPI and GO/R-SPI films

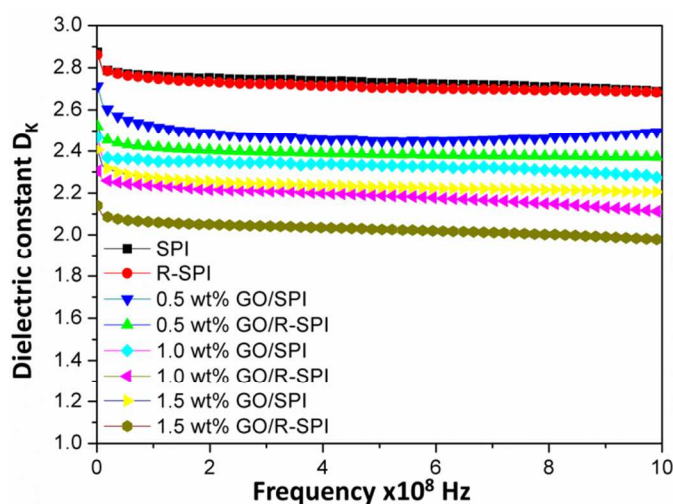


Fig. 10 Dielectric constant as a function of frequency for neat SPI and R-SPI films, and GO/SPI and GO/R-SPI films with various amounts of GO.

GO is an electrically insulating material, which contains oxygen randomly bonded to carbon on the graphene surface. The formation of these carbon–oxygen bonds results in the conversion of sp^2 -hybridized carbon atoms in graphite to sp^3 -hybridized carbon in GO. This process reduces the number of delocalized π -electrons, and disrupts the conjugated bond structure²³. To reduce the D_k value of PI, this study introduced GO sheets as interlayers in the SPI matrix, and these interlayers of insulating GO restricted electron mobility. Fig.10 exhibits the dielectric constants of the SPI and R-SPI films with increasing GO contents from 0.5 wt% to 1.5 wt%, over a frequency range of 0.01–1 GHz. Both the neat SPI and neat R-SPI films exhibited dielectric constants of approximately 2.8 at room temperature. These GO/SPI and GO/R-SPI films exhibited considerably lower dielectric constants than those of films that do not incorporate GO. The dielectric constants of the

GO/R-SPI composite films decreased steadily with an increase in the GO content, and a dielectric constant of approximately 2.1 was achieved for a GO content of 1.5 wt%. However, the 1.5 wt% GO/SPI film had a dielectric constant of approximately 2.3. The GO/R-SPI film with a 1.5 wt% GO content exhibited a greater decrease in the dielectric constant than that of the 1.5 wt% GO/SPI film. This result indicated that preparing the GO/R-SPI composite films by dissolving SPI to disperse GO, and then removing the solvent at 100 °C avoids a partial reduction of the oxygen-containing functional groups on the GO surface, thus maintaining the insulation properties of GO. This study demonstrates that the GO/R-SPI composite films with low D_k values meet the ILD requirement.

4. Conclusion

This study demonstrated an effective approach to prepare GO/R-SPI composite films as an alternative process to substitute the conventional fabrication methods of GO/SPI composites. The GO/R-SPI composite films possess a uniform crosslinking density. The dense SPI matrix structure provides an effective load transfer from the SPI matrix to the GO sheets. The 1.0 wt% GO/R-SPI composite film exhibited an increase of approximately 402% in tensile modulus, and 260% in tensile strength. The bulk dielectric constant was decreased from 2.8 for the neat SPI film to 2.1 for the 1.5 wt% GO/R-SPI composite film. This study provides a simple and effective method for fabricating GO-based PI composite materials with low D_k values and outstanding mechanical properties, and the performance of the 1.0 wt% and 1.5 wt% GO/R-SPI composites meets the current ILD requirements for ULSI multilevel interconnections.

Acknowledgements

This work was supported by Ministry of Science and Technology, Taipei, Taiwan, under Contract No. 103-2221-E-007-001-(103).

Notes

^aDepartment of Chemical Engineering, National Tsing Hua University, 101, Section 2, Kuang-Fu Road, Hsin-Chu, 30013, Taiwan. Fax: +886-3-571-5408; Tel: +886-3-571-3058; E-mail: ccma@che.nthu.edu.tw

References

1. G. Maier, *Prog. Polym. Sci.*, 2001, **26**, 3-65.
2. J.-Y. Wang, S.-Y. Yang, Y.-L. Huang, H.-W. Tien, W.-K. Chin and C.-C. M. Ma, *J. Mater. Chem.*, 2011, **21**, 13569-13575.
3. M. T. Bohr, Electron Devices Meeting, 1995. IEDM '95., International, 1995.
4. K. Maex, M. R. Baklanov, D. Shamiryan, F. Iacopi, S. H. Brongersma and Z. S. Yanovitskaya, *J. Appl. Phys.*, 2003, **93**, 8793-8841.
5. A. Allan, D. Edenfeld, W. H. Joyner, Jr., A. B. Kahng, M. Rodgers and Y. Zorian, *Computer*, 2002, **35**, 42-53.

6. G. Zhao, T. Ishizaka, H. Kasai, M. Hasegawa, T. Furukawa, H. Nakanishi and H. Oikawa, *Chem. Mater.*, 2008, **21**, 419-424.
7. A. R. Balkenende, F. K. de Theije and J. C. K. Kriege, *Adv. Mater.*, 2003, **15**, 139-143.
8. R. A. Pai, R. Humayun, M. T. Schulberg, A. Sengupta, J.-N. Sun and J. J. Watkins, *Science*, 2004, **303**, 507-510.
9. Y.-J. Lee, J.-M. Huang, S.-W. Kuo, J.-S. Lu and F.-C. Chang, *Polymer*, 2005, **46**, 173-181.
10. J. O. Simpson and A. K. St.Clair, *Thin Solid Films*, 1997, **308-309**, 480-485.
11. D. H. Wang, M. J. Arlen, J.-B. Baek and L.-S. Tan, *Macromolecules*, 2007, **40**, 6100-6111.
12. O.-K. Park, J.-Y. Hwang, M. Goh, J. H. Lee, B.-C. Ku and N.-H. You, *Macromolecules*, 2013, **46**, 3505-3511.
13. J. Longun and J. O. Iroh, *Carbon*, 2012, **50**, 1823-1832.
14. M. Yoonessi, Y. Shi, D. A. Scheiman, M. Lebron-Colon, D. M. Tigelaar, R. A. Weiss and M. A. Meador, *ACS Nano*, 2012, **6**, 7644-7655.
15. W.-H. Liao, S.-Y. Yang, J.-Y. Wang, H.-W. Tien, S.-T. Hsiao, Y.-S. Wang, S.-M. Li, C.-C. M. Ma and Y.-F. Wu, *ACS Appl Mater Interfaces*, 2013, **5**, 869-877.
16. I. S. Chung, C. E. Park, M. Ree and S. Y. Kim, *Chem. Mater.*, 2001, **13**, 2801-2806.
17. F. Mammeri, E. L. Bourhis, L. Rozes and C. Sanchez, *J. Mater. Chem.*, 2005, **15**, 3787-3811.
18. Y.-H. Zhang, Z.-M. Dang, S.-Y. Fu, J. H. Xin, J.-G. Deng, J. Wu, S. Yang, L.-F. Li and Q. Yan, *Chem. Phys. Lett.*, 2005, **401**, 553-557.
19. C.-M. Leu, G. M. Reddy, K.-H. Wei and C.-F. Shu, *Chem. Mater.*, 2003, **15**, 2261-2265.
20. S.-K. Lee, H. Y. Jang, S. Jang, E. Choi, B. H. Hong, J. Lee, S. Park and J.-H. Ahn, *Nano Lett.*, 2012, **12**, 3472-3476.
21. S. Stankovich, D. A. Dikin, G. H. B. Dommett, K. M. Kohlhaas, E. J. Zimney, E. A. Stach, R. D. Piner, S. T. Nguyen and R. S. Ruoff, *Nature*, 2006, **442**, 282-286.
22. Ramanathan T, A. A. Abdala, Stankovich S, D. A. Dikin, M. Herrera Alonso, R. D. Piner, D. H. Adamson, H. C. Schniepp, Chen X, R. S. Ruoff, S. T. Nguyen, I. A. Aksay, R. K. Prud'Homme and L. C. Brinson, *Nat Nano*, 2008, **3**, 327-331.
23. D. R. Dreyer, S. Park, C. W. Bielawski and R. S. Ruoff, *Chem Soc Rev*, 2010, **39**, 228-240.
24. X. Zhao, Q. Zhang, D. Chen and P. Lu, *Macromolecules*, 2010, **43**, 2357-2363.
25. C.-C. Teng, C.-C. M. Ma, C.-H. Lu, S.-Y. Yang, S.-H. Lee, M.-C. Hsiao, M.-Y. Yen, K.-C. Chiou and T.-M. Lee, *Carbon*, 2011, **49**, 5107-5116.
26. S. Wang, M. Tambraparni, J. Qiu, J. Tipton and D. Dean, *Macromolecules*, 2009, **42**, 5251-5255.
27. M. Abdalla, D. Dean, P. Robinson and E. Nyairo, *Polymer*, 2008, **49**, 3310-3317.
28. D. Liu, Z. Shi, M. Matsunaga and J. Yin, *Polymer*, 2006, **47**, 2918-2927.
29. W.-H. Liao, S.-Y. Yang, S.-T. Hsiao, Y.-S. Wang, S.-M. Li, C.-C. M. Ma, H.-W. Tien and S.-J. Zeng, *ACS Appl. Mater. Interfaces*, 2014, **6**, 15802-15812.
30. W. S. Hummers and R. E. Offeman, *J. Am. Chem. Soc.*, 1958, **80**, 1339-1339.
31. Y. Xu, H. Bai, G. Lu, C. Li and G. Shi, *J. Am. Chem. Soc.*, 2008, **130**, 5856-5857.
32. S. Stankovich, R. D. Piner, S. T. Nguyen and R. S. Ruoff, *Carbon*, 2006, **44**, 3342-3347.
33. T. I. T. Okpalugo, P. Papakonstantinou, H. Murphy, J. McLaughlin and N. M. D. Brown, *Carbon*, 2005, **43**, 153-161.
34. S.-Y. Yang, K.-H. Chang, H.-W. Tien, Y.-F. Lee, S.-M. Li, Y.-S. Wang, J.-Y. Wang, C.-C. M. Ma and C.-C. Hu, *J. Mater. Chem.*, 2011, **21**, 2374-2380.
35. S.-Y. Yang, C.-C. M. Ma, C.-C. Teng, Y.-W. Huang, S.-H. Liao, Y.-L. Huang, H.-W. Tien, T.-M. Lee and K.-C. Chiou, *Carbon*, 2010, **48**, 592-603.
36. M. Kotera, T. Nishino and K. Nakamae, *Polymer*, 2000, **41**, 3615-3619.
37. W.-H. Liao, H.-W. Tien, S.-T. Hsiao, S.-M. Li, Y.-S. Wang, Y.-L. Huang, S.-Y. Yang, C.-C. M. Ma and Y.-F. Wu, *ACS Appl Mater Interfaces*, 2013, **5**, 3975-3982.
38. I. H. Tseng, Y.-F. Liao, J.-C. Chiang and M.-H. Tsai, *MCP*, 2012, **136**, 247-253.

Graphical abstract

This study proposes a facile, practical and effective approach to prepare high-performance graphene oxide (GO)/ soluble polyimide (SPI) composite films through dissolved and dispersed strategy. In contrast with conventional procedure, this method can prevent the reduction of crosslinking reactions of the polymeric matrix, and maintain the existence of the oxygen-containing functional groups on GO, leading to the great improvements in the mechanical and dielectric properties.

